ANALYSIS OF A ROTATING DISK SYSTEM WITH AXIAL COOLING AIR

Z. Jiao **S. Fu***

School of Aerospace Engineering
Tsinghua University
Beijing, China

T. Kawakubo **S. Ohuchida** **H. Tamaki**

Products Development Center
IHI Corporation
Yokohama, Japan

ABSTRACT

In this article, a series of simulations of a rotating disk system with air cooling is introduced. These simulations are performed with the realizable k-ε eddy-viscosity model. Computational results illustrate the effect of the cooling air and disk rotation on the temperature of the disk surface. The maximum rotating disk speed reaches about 78300 rpm and the range of Reynolds numbers based on rotation speed is from about 0.7×10^6 to 3×10^6. The present work shows that the flow structure in the gap, which is on the opposite side of the cooling air, is rather similar to different cooling air flows. The temperature goes up as the rotating speed increases. The temperature in this gap will first decrease when the cooling air increases under lower mass flow rate. But when the cooling air continues to increase, the temperature will rise up indicating the existence of an optimum value of the cooling flow rate.

Keywords: Rotating disk, Air cooling, k-ε model, High rotating speed.

1. INTRODUCTION

Due to the ever-increasing demand for the efficiency and power of the compressor, the compressor impeller rotation speed is increased resulting in higher temperature, mechanical stress, serious unsteady phenomenon of the flow. In order to provide guidance and reference for the design and operation of the compressor, many numerical and experimental studies have been carried out on the flow phenomena in the surrounding area of the centrifugal compressor impeller. A simplified diagram of the centrifugal compressor is shown in Fig. 1.

The clearence between the impeller and the casing can be simplified into a rotor stator system like the schematic in Fig. 2.

Here b represents the outer radius of the disk, h is the width of the gap and Ω is the rotating speed of the rotor. Based on these basic parameters, there are two important dimensionless numbers that describe the rotating disk system:

$$G = \frac{h}{b} \tag{1}$$

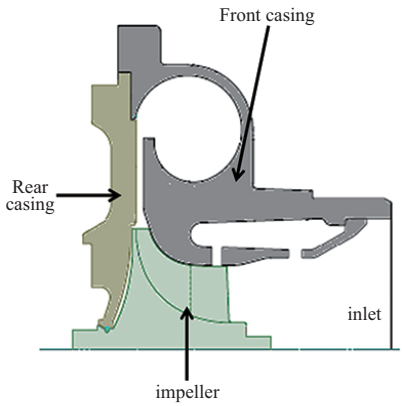


Fig. 1 Simplified diagram of a compressor.

$$\mathrm{Re}_\phi = \frac{\Omega b^2}{\nu} \tag{2}$$

G is called the aspect ratio and Re_ϕ is the rotation Reynolds number.

* Corresponding author (fs-dem@tsinghua.edu.cn)

DOI : 10.1017/jmech.2017.58
Copyright © 2017 The Society of Theoretical and Applied Mechanics
https://doi.org/10.1017/jmech.2017.58 Published online by Cambridge University Press

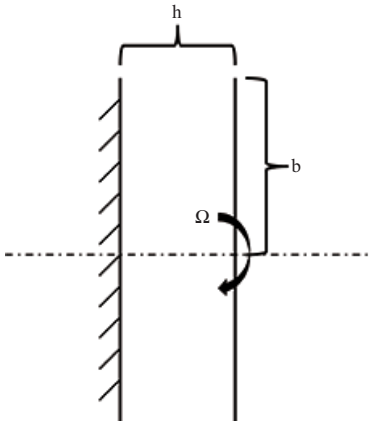


Fig. 2 Schematic of a rotor stator system.

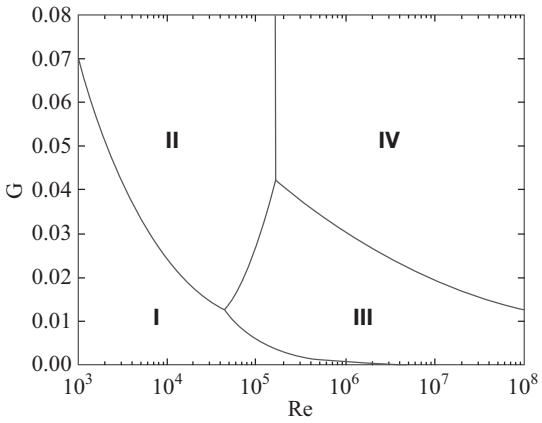


Fig. 3 Map of the four flow regions [4].

There had been many studies about rotating flows. The earlier research includes Ekman's study of the Ekman boundary layer [1] that is the boundary layer near the surface of the rotating disk. At the bottom of this boundary layer, the rotating speed of the fluid is the same as the rotating speed of the disk. The rotating speed outside the boundary layer is decreasing to zero, while the radial velocity of the fluid in the Ekman boundary layer is outward.

Bödewadt [2] studied fluid rotation on a stationary wall. The boundary layer here is called the Bödewadt boundary layer. At the bottom of the Bödewadt boundary layer, the velocity of the fluid is zero; outside the boundary layer, the rotating velocity is increasing from zero to the same speed of the main flow; the radial velocity of the fluid is centripetal in the Bödewadt boundary layer.

Batchelor [3] found that in the disk gap between these two boundary layers formed by two parallel disks with one rotating, there existed a solid body rotating core in which the radial and axial velocity gradients were nearly zero. The core rotating speed could be defined as KΩr with K called the core rotation coefficient.

Daily and Nece [4] studied the rotor-stator flow with G << 1, and summarized four basic flow regions in the gap, as shown in Fig. 3.

Based on the rotation Reynolds number and the aspect ratio, Daily and Nece divided the flow in the gap into four regions: I, the laminar flow with merged boundary layers; II, the laminar flow with separated boundary layers; III, the turbulent flow with merged boundary layers; IV, the turbulent flow with separated boundary layers. It can be seen that the main distinction between turbulence and laminar flow is the Reynolds number. Whether the two boundary layers are separated is mainly affected by the aspect ratio of the gap. In the case of separation of the boundary layers on both sides, there may be a solid body rotating core.

Debuchy *et. al* [5] have carried out detailed theoretical and experimental studies on the solid body rotating core, and determined the distribution range of the rotation coefficient K along the radius and the influence of the different outflow conditions on the rotating core.

In addition to the study of the flow field structures, the study of temperature and heat transfer in rotating flow has become a hot research topic as the rotating flow often occurs in high temperature and high pressure working environment.

Chen *et. al* [6] studied a rotating disk system with axial cooling flow both experimentally and numerically. Their results clearly showed the existence of a solid body rotating core between the rotating and stationary disks, and the temperature of the disk increases along the radius.

Roy *et. al* [7] also carried out experimental and numerical investigation on the rotor-stator system with Reynolds numbers ranging from 4.65×10^5 to 8.6×10^5. They mainly analyzed the temperature field and the convective heat transfer on the rotating disk surface. They considered the main flow rotation and the consequent secondary flow. Their results showed that the convective heat transfer coefficient is mainly affected by the secondary flow rate in the low-radius region, and it is mainly affected by rotation in the rotating core region at large radius. An empirical relation for the local Nusselt number distribution in the rotating core region was proposed. Yuan *et. al* [8] focused on the heat transfer on the stationary disk with slightly lower Reynolds numbers ranging from 1.42×10^5 to 3.33×10^5. They pointed out that there existed an optimal distance between the stationary and rotating disks offering the maximum heat transfer on the stationary disk. When the Reynolds number increases, the optimal distance decreases. Boutarfa and Harmand [9] in their study obtained an empirical relation about the local Nusselt number, the rotation Reynolds number and the gap aspect ratio.

Pellé and Harmand [10] carried out an experiment on the flow-side temperature distribution with axial cooling flow. They showed that the temperature distribution was divided into two regions: at small radius it was mainly affected by the jet flow while at large radius it was affected by the speed and flow cooling effect.

Wang and Wilson [11] computed the rotating flow of a flywheel structure. WRÓBLEWSKI and FRĄCZEK [12] studied numerically the heat transfer of the rotating flow in in the axial compressor. Their results showed good agreement between numerical simulations with SST *k-ω* model and experimental results for a rotating

https://doi.org/10.1017/jmech.2017.58 Published online by Cambridge University Press

flow with complex structures.

The current study aims at a detailed understanding of the flow field in the high speed impeller disk cavity and its resulting thermal field, typical of high pressure ratio centrifugal compressors. The impeller is simplified into a rotating disk in the experiments and simulations. The main objective is to analyze the influence of the disk rotating speed and the cooling effect of the axial incoming cooling air to this rotating disk system.

2. SIMULATION DETEILS

In order to analyse the rotating flow near the centrifugal compressor impeller, an experimental apparatus was built. The schematic is shown in Fig. 4. The rotating disk diameter is 146 mm. Sensors are placed on the steel casing to measure temperature and pressure. The cavity or the space on the left side of the rotor is 2 mm wide and the right side cavity is 5 mm wide that is also the passage of cooling air.

According to this apparatus, axisymmetric mesh topology is created for the axisymmetric simulations. Figure 5 shows, schematically, the main components around the rotating disk (the rotor) including the stationary casing. The bottom line of Fig. 5 coincides with the axis of rotation.

The flow inside the left and right cavities and the temperature variations of the casing are calculated simultaneously with the help of FLUENT code. Three different mesh densities, 1.5, 2.38 and 3 million grid nodes, respectively are generated to insure grid independence. These grids are referred to No.1, No.2 and No.3 mesh. More nodes are arranged in the fluid than in the solid regions, especially in the region adjacent to the wall to ensure that the y^+ for the first layer is less than one. Figure 6 is a focused view of the mesh at the top cavity region on the LHS of the rotor.

Computational results show that the three grid meshes provide very similar results as seen in Fig. 7 where velocity and temperature distributions are exhibited. It suggests that the coarse grid employed here is fine enough to give satisfactory results.

The fluid in the present computation is set as a compressible ideal gas. The calculation formulations are implicit, and Roe scheme is chosen. The wall boundary is set non-slip. At the inner boundary between the fluid region and solid region, the temperature and heat flux will be calculated in couple. The outside boundary condition is convective. The mass flow rate at the inlet and the rotation speed of the disk are set respectively.

Cooper and Reshotko [13] point that the flow transition of the rotor stator system occurs when the local Reynolds number is within 1.6×10^5 to 2.5×10^5. Under the conditions in this article, it may occur at very low radius region. So the transition is not considered in this article. Considering about the rotation of the main flow and the considerable second flow, the realizable k-ε model [14] are chosen for the simulations.

It can be proved that the realizable k-ε model is suitable for the simulation. The result of velocity compo-

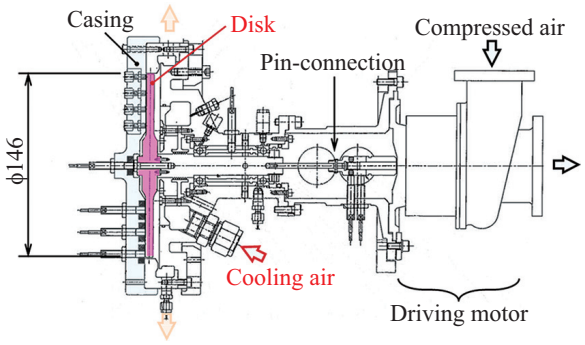


Fig. 4 Schematic of the experiment apparatus.

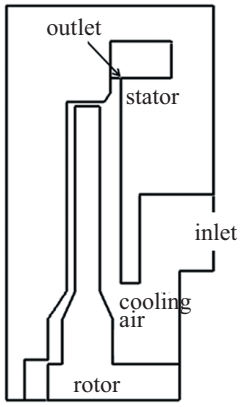


Fig. 5 The axisymmetric topology of the computational domain including rotor, cavities and solid casing regions.

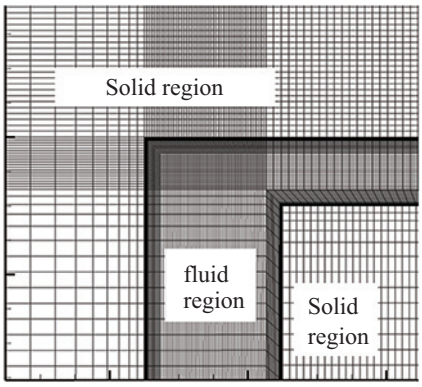


Fig. 6 Focused view of the grid arrangement at top cavity region on the LHS of the rotor.

nents between Chen's study [6] and the validation case with realizable k-ε model is shown in Fig. 8. In this case, the rotating speed is about 126 rad/s and cooling air mass flow rate is about 0.042 kg/s. In Fig. 8, comparing with Chen's simulation results, the simulations with realizable k-ε model match better with the experiment data of both the radial velocity and the tangential velocity in the core region. In Fig. 8(a) and Fig. 8(b), the current simulations with realizable k-ε model get the negative value of radial velocity near the stator success-

https://doi.org/10.1017/jmech.2017.58 Published online by Cambridge University Press

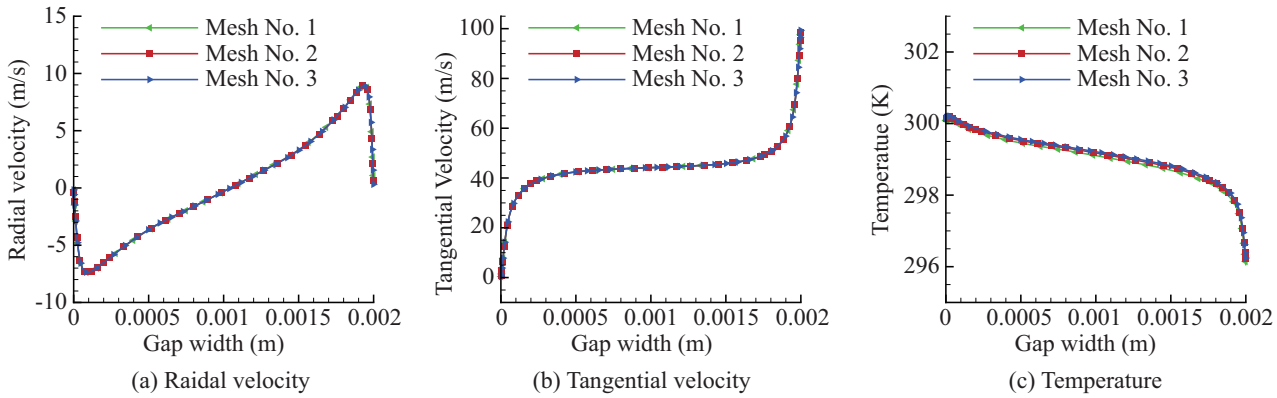


Fig. 7 Sub-name's order should be (a) radial velocity; (b) tangential velocity; (c) temperature.

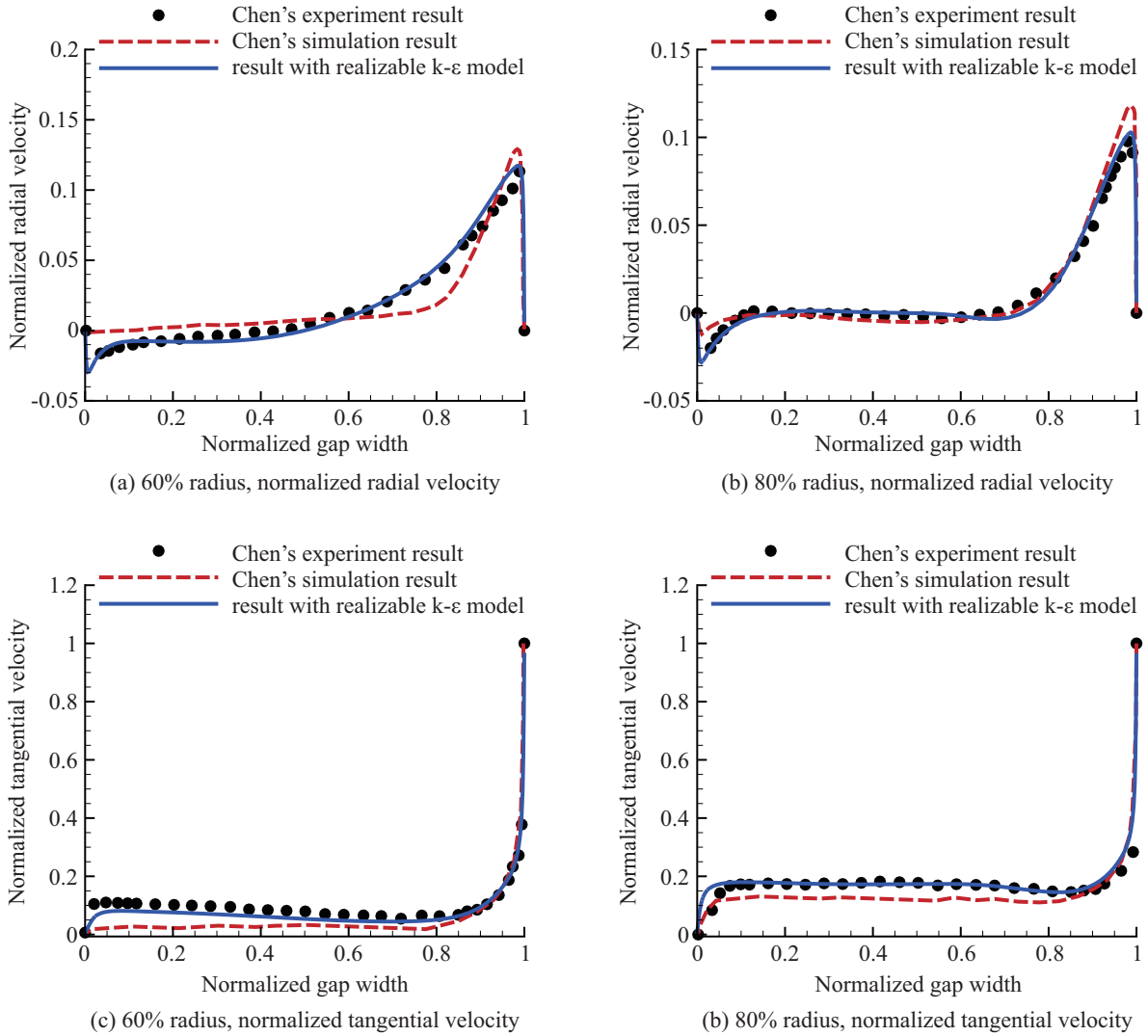


Fig. 8 Comparison between Chen's experiment results and validation case of k-ε model.

fully which occurs in the experiments and doesn't occur in Chen's simulation result and get a better match of the maximum radial velocity in the boundary layer close to rotor. In Fig. 8(c) and Fig. 8(d), the current simulations with realizable k-ε model also get a better match of the tangential velocity in the boundary layers close to both sides under large gradient. It reveals that the current simulation with realizable k-ε model is valid.

https://doi.org/10.1017/jmech.2017.58 Published online by Cambridge University Press

Table 1 Conditions with stable mass flow rate of case 1

	Mass flow rate (kg/s)	Periphery speed(m/s)	Re_ϕ
Case 1-1	0.02998	208	1.02×10^6
Case 1-2	0.02994	233	1.14×10^6
Case 1-3	0.02949	252	1.23×10^6
Case 1-4	0.02945	276	1.35×10^6
Case 1-5	0.02904	299	1.46×10^6
Case 1-6	0.02944	325	1.59×10^6
Case 1-7	0.02903	346	1.70×10^6
Case 1-8	0.02908	369	1.81×10^6
Case 1-9	0.02885	387	1.90×10^6

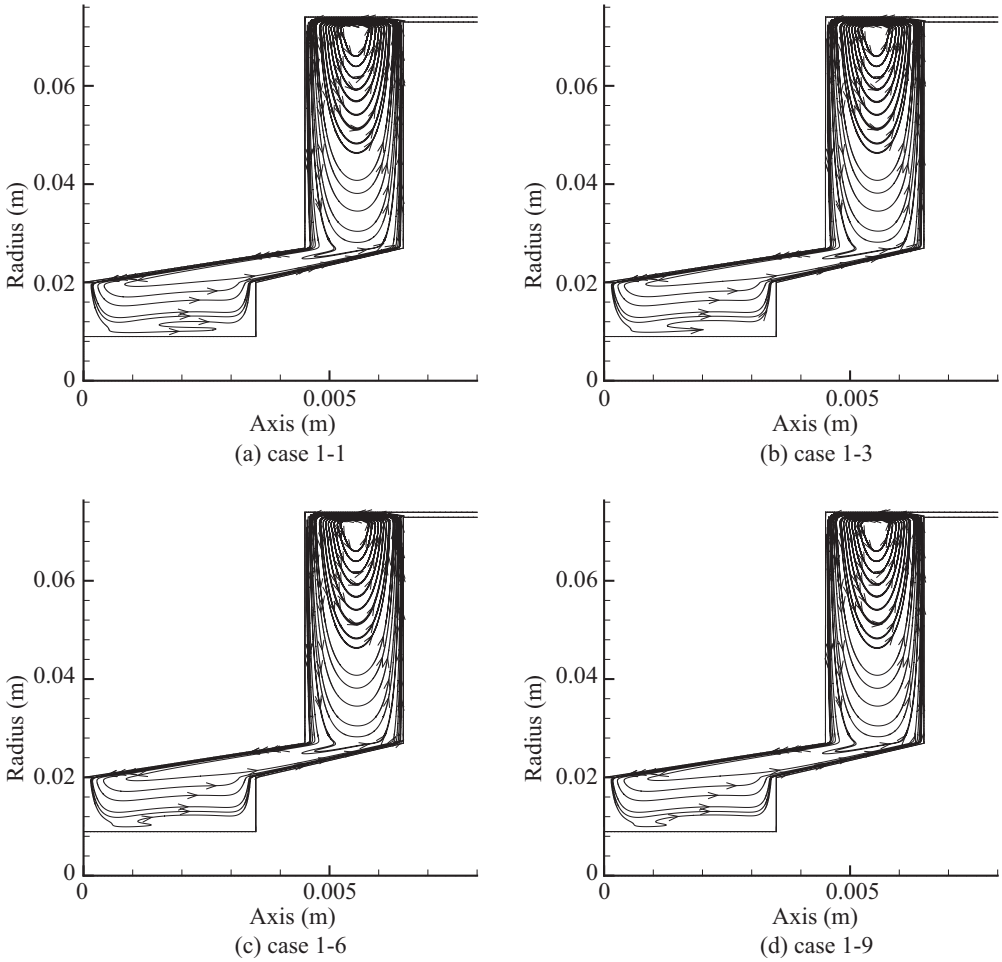


Fig. 9 Streamlines of the results of case 1.

3. RESULTS AND DISCUSSIONS

3.1 Effect of Disk Rotating Speed

In this article, a series of experiment and simulation is done to analyze the effect of the rotating speed and cooling air mass flow rate. Table 1 lists different cases in which the mass flow rate is kept basically unchanged while the rotating speed increases. For intuitive comparison, the periphery speed (ΩR, R = 73 mm) of the rotating disk is used to represent the speed of rotation.

Figure 9 shows the simulation results of streamlines in the left gap of case 1-1, case 1-3, case1-6 and case 1-9 (For ease of observation, the x-coordinate is magnified by a factor of ten). It reveals that the structures in the left gap of the cases are similar when the disk rotating speed increases. There is a big circulation filled with the entire gap. The flow moves outwards along the

https://doi.org/10.1017/jmech.2017.58 Published online by Cambridge University Press

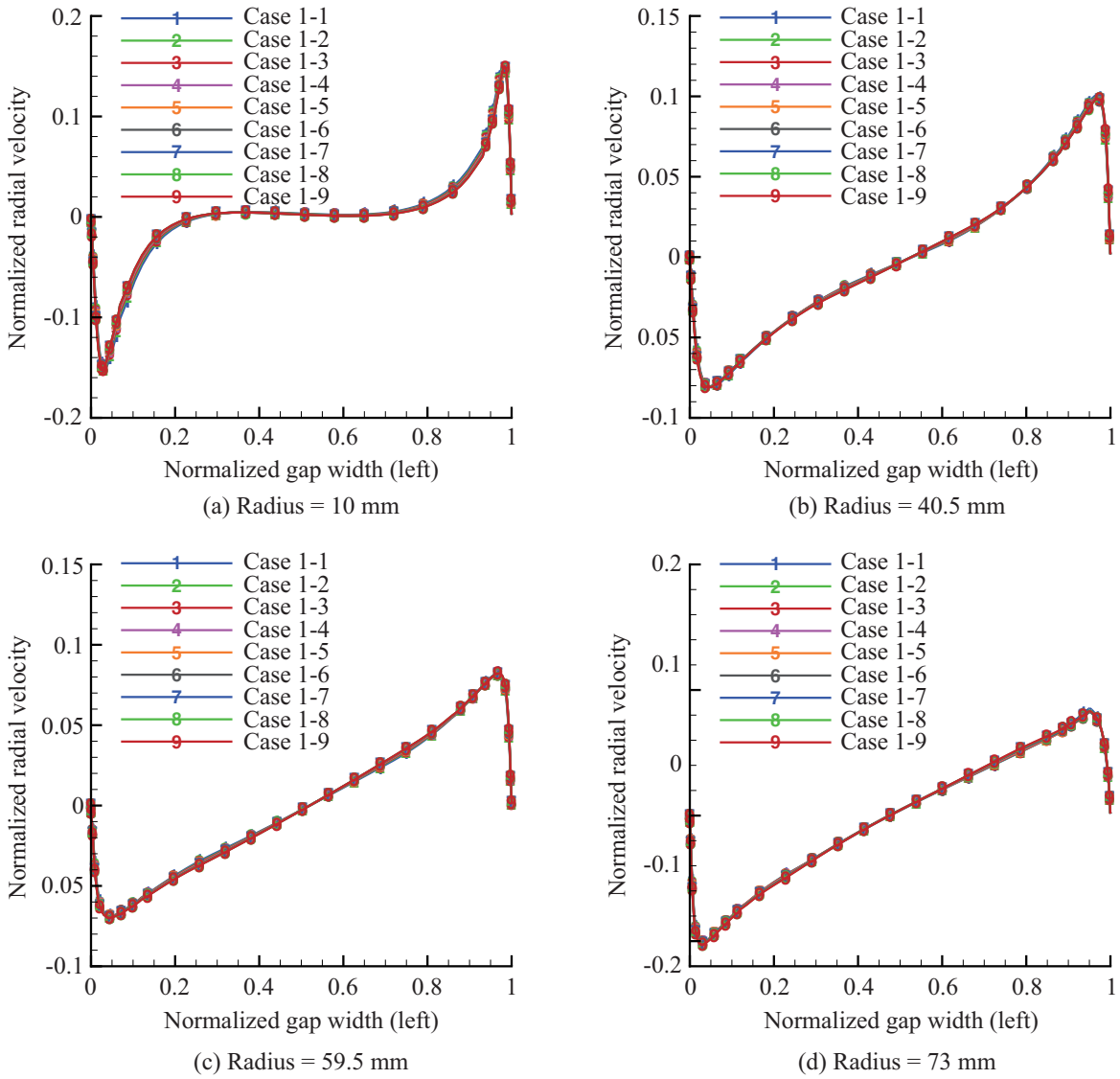


Fig. 10 Axial distributions of normalized radial velocity in left gap of case 1.

rotating disk and moves inwards along the stationary casing after being bended at the periphery. Then it moves from the stationary casing to the rotating disk so that form the entire circulation. The center of the circulation is very close to the periphery of the gap.

The velocity components U can be normalized in this way:

$$U^* = U / \Omega r \tag{3}$$

where U^* is often called reduced velocity.

Figures 10, 11 and Fig. 12 show profiles of distribution of normalized velocity components at different radii in left gap. The radius of 73 mm is at the periphery of the disk and the radius of 10 mm is close to the hub. The normalized velocity components show approximately similar profile among the cases. It reveals that the normalized structure the in left gap is similar. Comparing with the other two components, the axial component is very small. It significantly shows that the axial velocity reverses at periphery comparing with the three other radial positions because this position is above the center of the circulation structure. The approximate symmetric shape of the radial velocity component confirms the existence of the circulation structure. The tangential velocity component shows that at the middle of the gap, the fluid has a similar tangential velocity in the axial direction. It forms a not obvious solid body rotating core.

For the group of case 1, the temperature inside the left gap at four different radii is measured. The comparison between measured data and axial average values of the simulations are shown in Fig. 13. Although there are differences between the simulation and experiment, they have the same trends. The temperature increases when the disk rotating speed goes up. This is easy to explain, because in this system the main source of energy is the rotation of the disk, which generates heat by friction. It can be considered to continue to increase the disk rotating speed, the temperature will rise further.

https://doi.org/10.1017/jmech.2017.58 Published online by Cambridge University Press

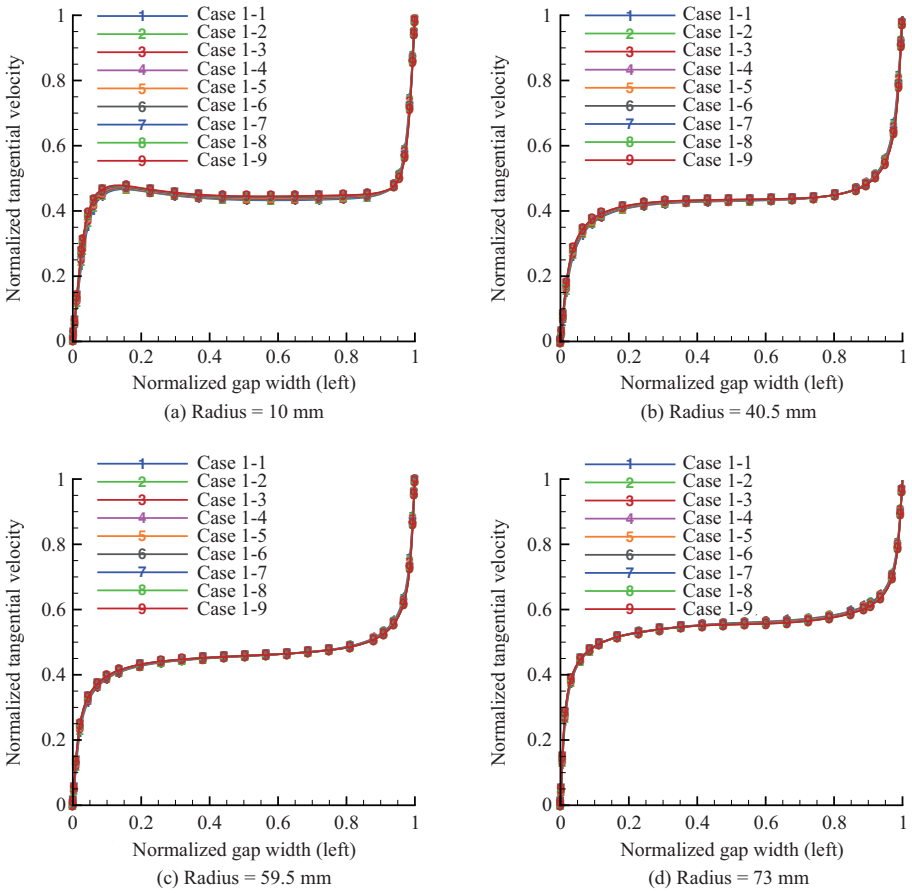


Fig. 11 Axial distributions of normalized tangential velocity in left gap of case 1.

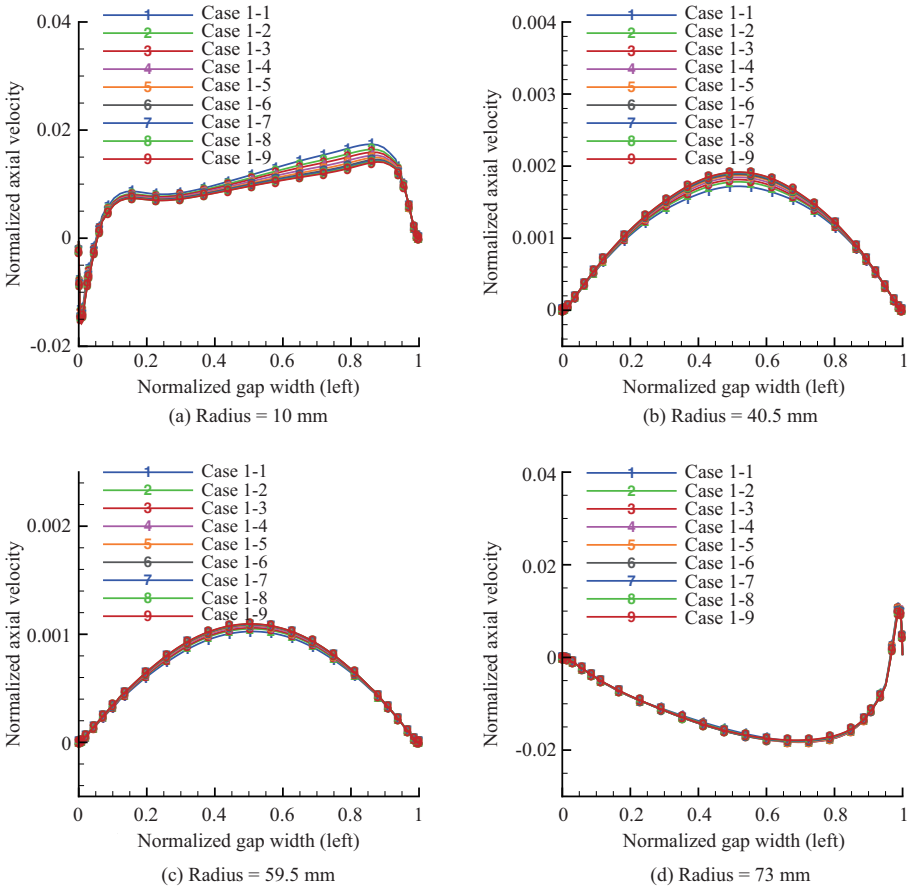


Fig. 12 Axial distributions of normalized axial velocity in left gap of case 1.

https://doi.org/10.1017/jmech.2017.58 Published online by Cambridge University Press

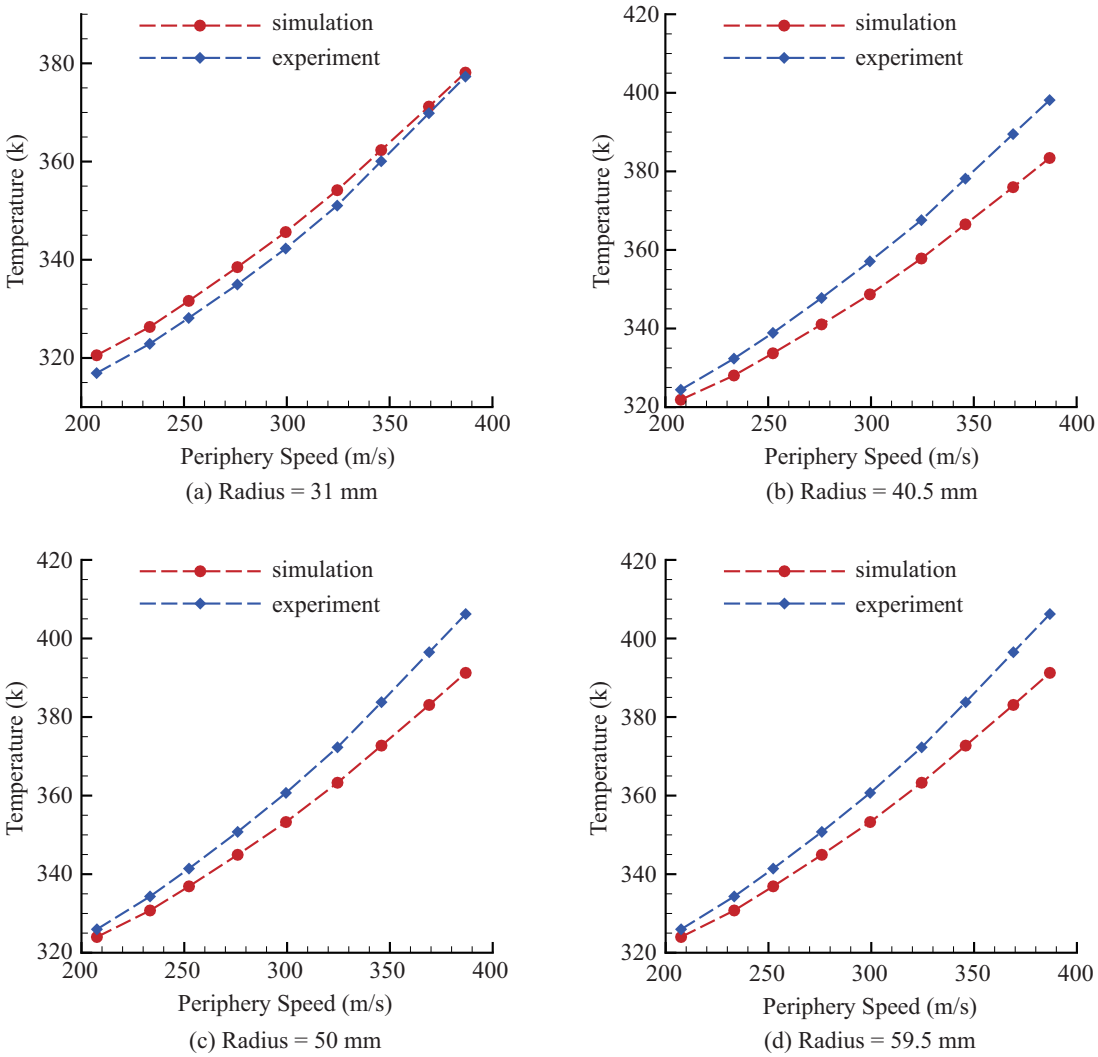


Fig. 13 Temperature comparison between experiments and simulations of case 1.

Table 2 Conditions with same disk rotating speed of case 2

	Mass flow rate (kg/s)	Periphery speed(m/s)	Re_ϕ
Case 2-1	0.1	600	2.94×10^6
Case 2-2	0.2	600	2.94×10^6
Case 2-3	0.3	600	2.94×10^6
Case 2-4	0.4	600	2.94×10^6
Case 2-5	0.5	600	2.94×10^6
Case 2-6	0.6	600	2.94×10^6

3.2 Effect of Mass Flow Rate of the Cooling Air

Another group of cases is carried out to explore the effects of cooling air flow rate. Their conditions are listed in Table 2.

The streamlines of the flow structure in the left gap are shown in Fig. 14. It can be seen that the structure keeps similar like case 1 while the mass flow rate increases.

The profiles of distribution of the normalized velocity component at different radius in the left gap are presented in Figs. 15, 16 and Fig. 17. Despite minor differences, the profiles of each case are similar substantially which validates the results in Fig. 14. Since the rotating speed of these cases is the same, it means that the velocity components are also similar.

It can be seen that the flow structure and velocity profiles of group 1 and group 2 are very similar. It indicates that the normalized flow field inside the left gap is approximately uniform.

https://doi.org/10.1017/jmech.2017.58 Published online by Cambridge University Press

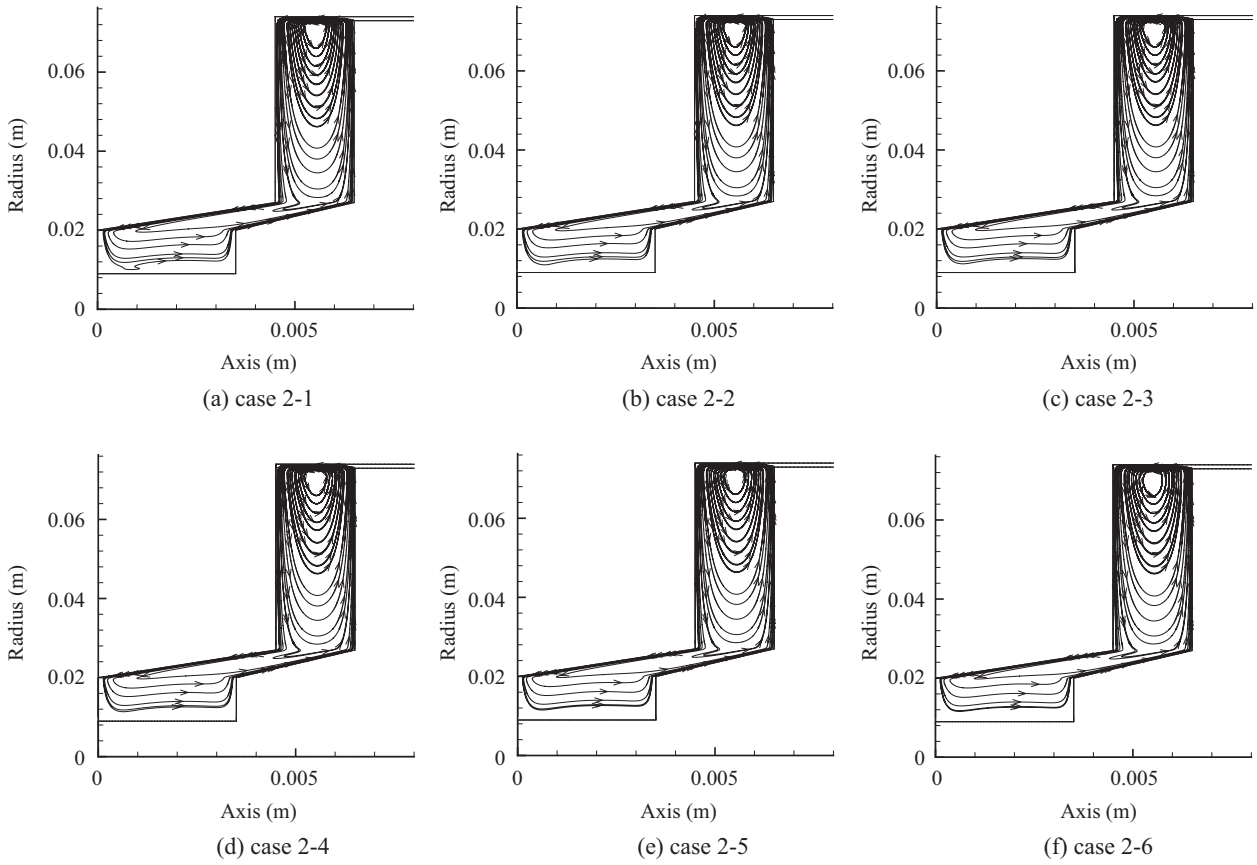


Fig. 14 Streamlines of the results of case 2.

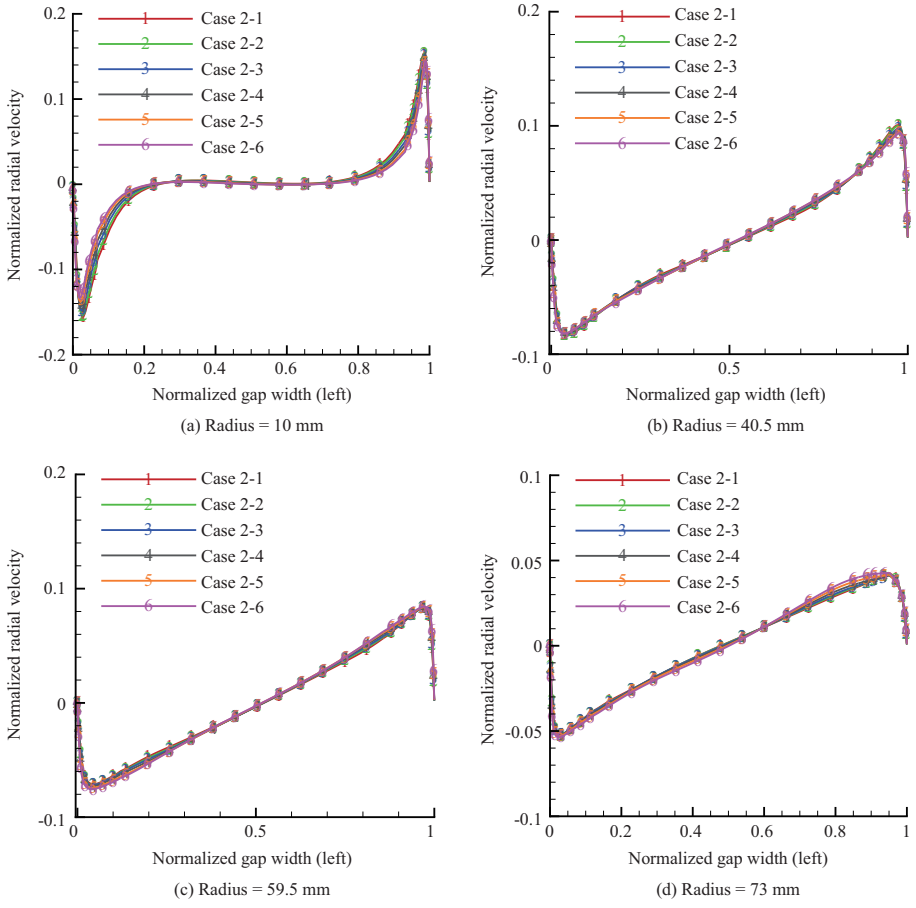


Fig. 15 Axial distributions of normalized radial velocity in the left gap of case 2.

https://doi.org/10.1017/jmech.2017.58 Published online by Cambridge University Press

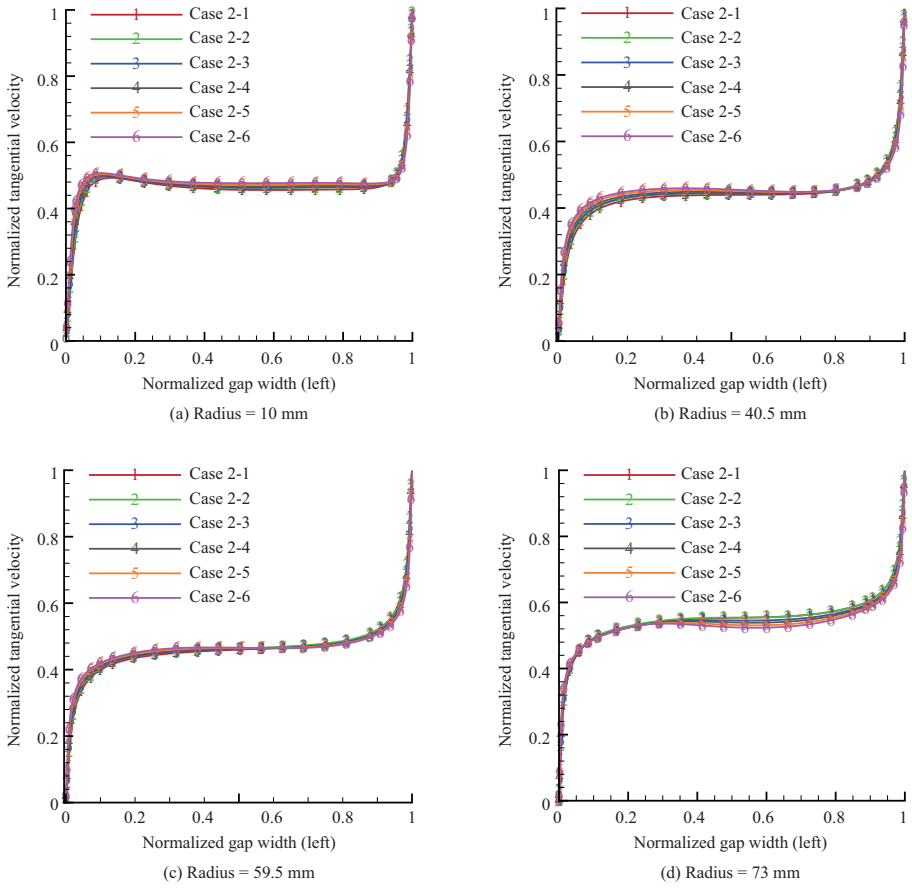


Fig. 16 Axial distributions of normalized tangential velocity in the left gap of case 2.

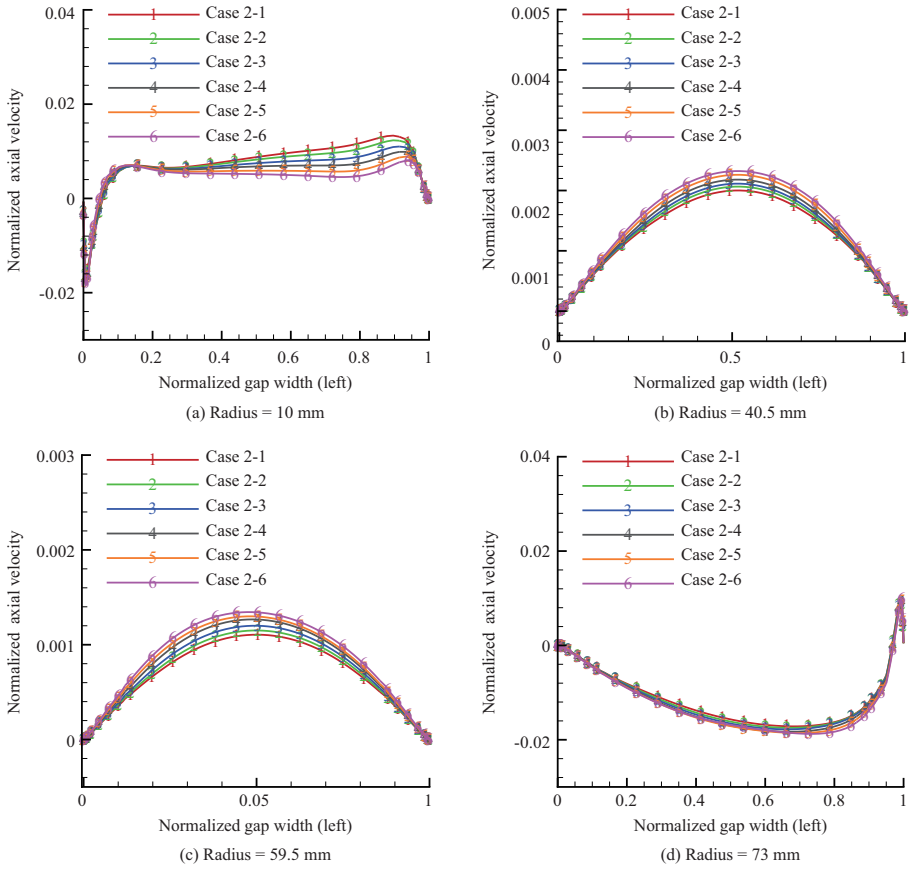


Fig. 17 Axial distributions of normalized axial velocity in the left gap of case 2.

https://doi.org/10.1017/jmech.2017.58 Published online by Cambridge University Press

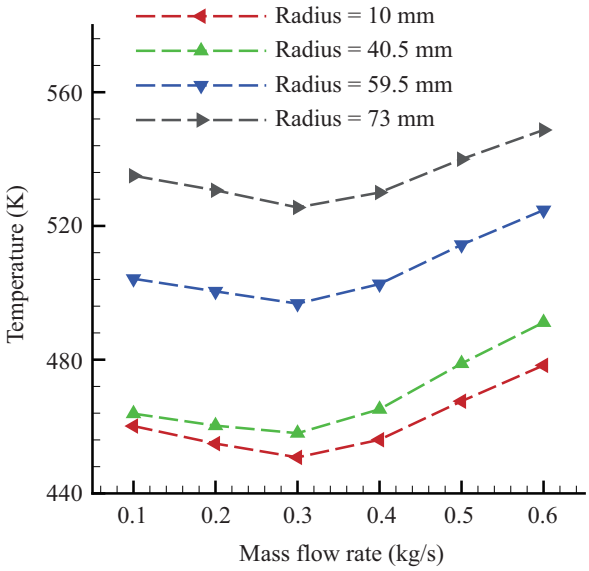


Fig. 18 Axial average temperature in the left gap of case 2.

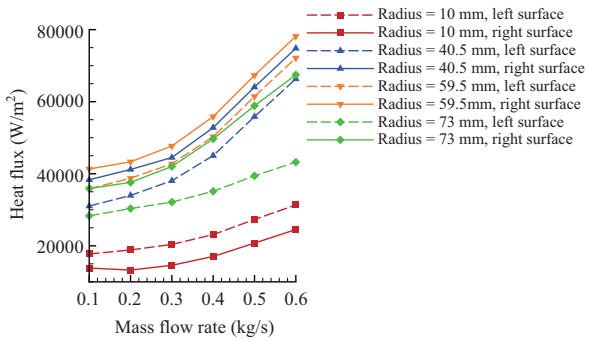


Fig. 19 Magnitude of the surface heat flux of case 2.

Figure 18 shows the results of the axial average temperature for the six different cases in the left gap at different radii. In general, the purpose of increasing the cooling air rate is to reduce the temperature. It works from case 2-1 to case 2-3, but fails in case 2-4, 2-5 and 2-6. From case 2-4 to 2-6, the temperature did not decline but increased.

Temperature should be the result of the balance of the heat generation and transport. In this rotating disk system, the heat transport is mainly caused by the cooling air. The heat mainly transports through the solid casing and disk, and will be taken away by the air. The heat generation is mainly caused by the shear stress inside the fluid region, including the friction on the solid surface.

The strength of the heat transport can be represented by the magnitude of the heat flux through the casing surface. Figure 19 shows the magnitude of the surface heat flux on both side of the disk at four different radii. It indicates that the heat flux magnitude at higher radius is higher than lower position. The flux on the right surface is higher than the left surface at three higher radii. The most important is that the heat flux magnitude is increasing when the cooling air mass flow rate increases.

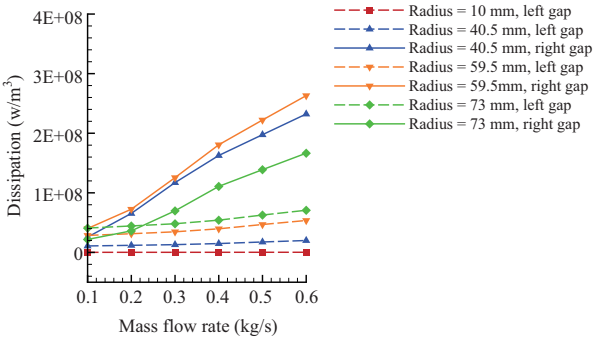


Fig. 20 Axial average values of the dissipation of case 2.

This is consistent with the purpose of increasing the cooling air.

On the other hand, the transport equation of internal energy is listed below:

$$\frac{\partial e}{\partial t}+V\cdot\nabla e=-\frac{P}{\rho}\nabla\cdot V+\frac{\Phi}{\rho}+Q \tag{4}$$

Φ is the dissipation function:

$$\Phi=-\frac{2}{3}\mu(u_{i,i})^2+2\mu S_{ij}S_{ij} \tag{5}$$

It can represent the intensity of the heat generation per volume.

The axial average values of the dissipation in both the left and right gap at four radii of the six cases are shown in Fig. 20. Since it connects to the inlet of the cooling air at radius of 10mm in the right gap, it is hard to define the average value here. So it is not presented in Fig. 20. It reveals that the dissipation is also increasing as the cooling air increases. In the right gap, the dissipation is larger and increasing faster than the left gap.

By taking case 2-1 as a reference, the dissipation and heat flux magnitude can be normalized as below:

$$X^*=\frac{X_i}{X_{ref}} \tag{6}$$

where X^* presents the normalized value of each parameter, X_{ref} is the value in case 2-1, X_i is the value in each case.

The comparison of normalized dissipation and heat flux magnitude is shown in Fig. 21. It indicates that both the dissipation and heat flux magnitude is increasing while the cooling air flow rate increases. The heat flux magnitude of both side of the disk and the dissipation in the left gap are increasing at a similar rate. The dissipation in the right gap is increasing faster than others.

At low cooling flow rate, the effect of the heat transport is greater than the heat generation. The cooling effect dominates the temperature, so the temperature is decreasing. As the cooling air flow rate increasing, the heat generation is growing faster. At higher flow rate, the effect of heat generation exceeds the heat transport. So the temperature is increasing from this time.

https://doi.org/10.1017/jmech.2017.58 Published online by Cambridge University Press

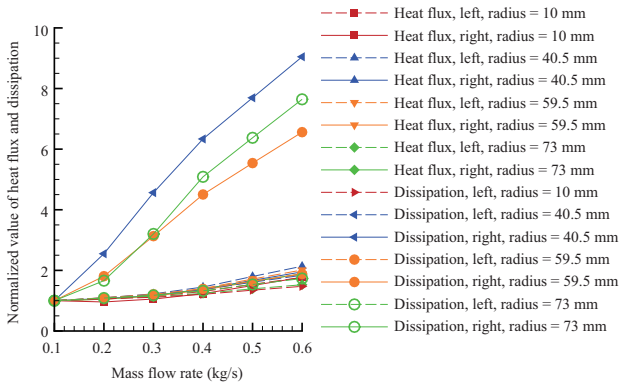


Fig. 21 Comparison between the normalized value of dissipation and magnitude of heat flux of case 2.

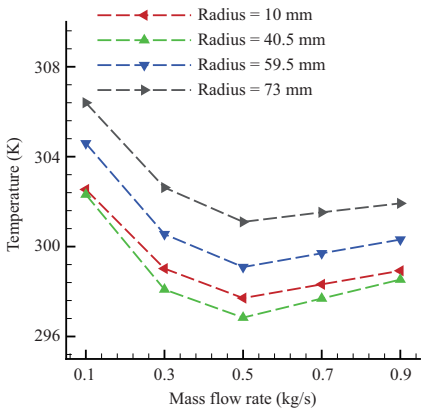


Fig. 22 Axial average temperature of case 3.

Table 3 Conditions with same disk rotating speed of case 3

	Mass flow rate (kg/s)	Periphery speed(m/s)	Re_ϕ
Case 3-1	0.1	146	0.715×10^6
Case 3-2	0.3	146	0.715×10^6
Case 3-3	0.5	146	0.715×10^6
Case 3-4	0.7	146	0.715×10^6
Case 3-5	0.9	146	0.715×10^6

One more group under lower rotating speed with different cooling air rate is listed in Table. 3. The results of the axial average temperature for this group in the left gap at four different radii are shown in Fig. 22. The temperature is still decreasing under lower cooling air flow rate and will begin to rise up while the cooling air continues to increase. It confirms the conclusion of group 2.

4. CONCLUSIONS

In this article a system of a rotating disk with axial coming cooling air is simulated. The effects of the disk rotation and cooling air flow rate to the flow structure and temperature in the rear gap between the disk and the stationary casing at the opposite side of the cooling air are mainly discussed.

It reveals that in the rotation Reynolds number range of 0.7×10^6 to 3×10^6, the flow structure in the rear gap remains similar. There is a big circulation structure. Either of the radial, tangential and axial velocity components is symmetrical or centrally symmetrical.

It is clear that the rotation dominates the disk temperature. The temperature will increase as the rotational speed increases. The target of cooling air is to cool the disk and this works well at low mass flow rate. The results show that the heat transport by the heat flux through the disk surface will increase as the cooling air mass flow rate increases.

There is a limit in the mass flow rate of the cooling air above which further increase of the cooling air will raise, rather than reduce, the temperature of the disk. The simulation results show that both the heat generation and heat transfer will increase as the cooling air flow rate increase. The heat generation increased faster than the heat transfer under large mass flow rate. As a result, the temperature will increase when the cooling air flow rate exceeds the limit value.

ACKNOWLEDGEMENTS

This work is supported by IHI Corporation. The authors are particularly thankful to Prof. Qibing Li for valuable discussions and suggestions.

REFERENCES

1. Ekman, V. W., "Om Jordrotationens Inverkan p˚a Vindstrømmar I Hafvet," *Nytt Magasin for Naturvidenskapene*, **40**, pp. 37-62 (1902).
2. Bödewadt, U. T., "Die Drehströmung über Festem Grunde," *Zeitschrift für Angewandte Mathematik und Mechanik*, **20**, pp. 241-253 (1940).
3. Batchelor, G. K., "Note on a Class of Solutions of the Navier-Stokes Equations Representing Steady Rotationally Symmetric Flow," *Quarterly Journal of Mechanics and Applied Mathematics*, **4**, pp. 29-41 (1951).

https://doi.org/10.1017/jmech.2017.58 Published online by Cambridge University Press

4. Daily, J.W. and Nece, R. E., "Chamber Dimension Effects on Induced Flow and Frictional Resistance of Enclosed Rotating Disks," *Journal of Basic Engineering*, **82**, pp. 217-232 (1960).
5. Debuchy, R., Nour, F. A. and Bois, G., "An Analytical Modeling of the Central Core Flow in a Rotor-Stator System with Several Preswirl Conditions," *Journal of Fluids Engineering*, **132**, 061102 (2010).
6. Chen, J. X., Gan, X. P. and Owen, J. M., "Heat Transfer in an Air-Cooled Rotor-Stator System," *Journal of Turbomachinery*, **118**, pp. 444-451 (1996).
7. Roy, R. P., Xu, G. and Feng, J., "A Study of Convective Heat Transfer in a Model Rotor-Stator Disk Cavity," *Journal of Turbomachinery*, **123**, pp. 621-632 (2001).
8. Yuan, Z. X., Saniei, N. and Yan, X. T., "Turbulent Heat Transfer on the Stationary Disk in a Rotor-Stator System," *International Journal of Heat and Mass Transfer*, **46**, pp. 2207-2218 (2003).
9. Boutarfa, R. and Harmand, S., "Local Convective Heat Exchanges and Flow Structure in a Rotor-Stator System," *International Journal of Thermal Sciences*, **42**, pp. 1129-1143 (2003).
10. Pellé, J. and Harmand, S., "Heat Transfer Study in a Rotor-Stator System Air-Gap with an Axial Inflow," *Applied Thermal Engineering*, **29**, pp. 1532-1543 (2009).
11. Wang, L. and Wilson, M., "Computations of Flow and Heat Transfer in a Rotor Stator System with Externally-Induced Ingestion," *International Journal of Gas Turbine, Propulsion and Power Systems*, **1**, pp. 10-18 (2012).
12. Wróblewski, W. and Frączek, D., "Heat Transfer Modelling in a Rotating Cavity Using the SST k-ω Turbulence Model," *Archives of Mechanics*, **66**, pp. 343-364 (2014).
13. Cooper, P. and Reshotko, E., "Turbulent Flow Between a Rotating Disk and a Parallel Wall," *AIAA Journal*, **13**, pp. 573-578 (1975).
14. Shih, T. H., Liou, W. W., Shabbir, A., Yang, Z. and Zhu, J., "A New K-ε Eddy-Viscosity Model for High Reynolds Number Turbulent Flows - Model Development and Validation," *Computers Fluids*, **24**, pp. 227-238 (1995).

(Manuscript received February 6, 2017,
accepted for publication May 30, 2017.)

https://doi.org/10.1017/jmech.2017.58 Published online by Cambridge University Press